

Constraining the redshifted 21-cm signal with the unresolved soft X-ray background

Anastasia Fialkov^{1,2*}, Aviad Cohen³, Rennan Barkana^{3,4,5,6} & Joseph Silk^{5,7,8}

¹ *Harvard-Smithsonian Center for Astrophysics, Institute for Theory and Computation, 60 Garden Street, Cambridge, MA 02138, USA*

² *Département de Physique, Ecole Normale Supérieure, CNRS, 24 rue Lhomond, Paris, 75005 France*

³ *Raymond and Beverly Sackler School of Physics and Astronomy, Tel Aviv University, Tel Aviv 69978, Israel*

⁴ *Sorbonne Universités, Institut Lagrange de Paris (ILP), Institut d’Astrophysique de Paris, UPMC Univ Paris 06/CNRS*

⁵ *Department of Astrophysics, University of Oxford, Denys Wilkinson Building, Keble Road, Oxford OX1 3RH, UK*

⁶ *Perimeter Institute for Theoretical Physics, 31 Caroline St N., Waterloo, ON N2L 2Y5, Canada*

⁷ *Department of Physics and Astronomy, The Johns Hopkins University, Baltimore, MD 21218, USA*

⁸ *Sorbonne Universités, UPMC Univ Paris 6 et CNRS, UMR 7095, Institut d’Astrophysique de Paris, 98 bis bd Arago, 75014 Paris, France*

26 October 2016

ABSTRACT

We use the observed unresolved cosmic X-ray background (CXRB) in the 0.5 – 2 keV band and existing upper limits on the 21-cm power spectrum to constrain the high-redshift population of X-ray sources, focusing on their effect on the thermal history of the Universe and the cosmic 21-cm signal. Because the properties of these sources are poorly constrained, we consider hot gas, X-ray binaries and mini-quasars (i.e., sources with soft or hard X-ray spectra) as possible candidates. We find that (1) the soft-band CXRB sets an upper limit on the X-ray efficiency of sources that existed before the end of reionization, which is one-to-two orders of magnitude higher than typically assumed efficiencies, (2) hard sources are more effective in generating the CXRB than the soft ones, (3) the commonly-assumed limit of saturated heating is not valid during the first half of reionization in the case of hard sources, with any allowed value of X-ray efficiency, (4) the maximal allowed X-ray efficiency sets a lower limit on the depth of the absorption trough in the global 21-cm signal and an upper limit on the height of the emission peak, while in the 21-cm power spectrum it sets a minimum amplitude and frequency for the high-redshift peaks, and (5) the existing upper limit on the 21-cm power spectrum sets a lower limit on the X-ray efficiency for each model. When combined with the 21-cm global signal, the CXRB will be useful for breaking degeneracies and helping constrain the nature of high-redshift heating sources.

Key words: cosmology: dark ages, reionization, first stars – X-rays: diffuse background – cosmology: theory

1 INTRODUCTION

The cosmic X-ray background (CXRB) was the first cosmic background radiation to be discovered (Giacconi et al. 1962); however, its origin is not fully understood yet. Deep extragalactic X-ray surveys have resolved $\approx 76 - 88\%$ of the CXRB into point sources, with the resolved fraction increasing at higher energies (Lehmer et al. 2012). It is now clear that the resolved CXRB is mostly produced by the integrated emission from Active Galactic Nuclei (AGN) at $z \leq 8$ and galaxies located at redshifts out to $z = 2.6$ (Lehmer et al. 2012). However, a part of the CXRB remains unresolved and its origin is still undetermined. The largest fraction of the unresolved CXRB is in the soft (0.5 – 2

keV) band, which has been explored by a number of X-ray missions (McCammon et al. 2002; Hickox & Markevich 2006; Lehmer et al. 2012); the unresolved fraction is 24.3% of the total $8.15 \pm 0.58 \times 10^{-12} \text{ erg cm}^{-2}\text{s}^{-1}\text{deg}^{-2}$ background measured by *Chandra* (Lehmer et al. 2012) in this band. Future missions such as the proposed X-ray Surveyor (Weisskopf et al. 2015) and Athena¹ should be able to resolve this fraction, thus further constraining the contribution of distant and faint X-ray sources.

At present, the nature of the unresolved fraction of the CXRB is still debated. On the one hand, measurements of the X-ray background hint that in the soft band normal galaxies may play an increasingly important role (Xue et al.

* E-mail: anastasia.fialkov@cfa.harvard.edu

¹ <http://www.the-athena-x-ray-observatory.eu/>

2011), likely dominating over AGN at fluxes below the detection limit of *Chandra* ($\sim 5 \times 10^{-18}$ erg cm $^{-2}$ s $^{-1}$ in this band). Extrapolating the available data, Bauer et al. (2004) predicted that the number density of star-forming galaxies should overtake that of AGN at fluxes just below $\sim 1 \times 10^{-17}$ erg cm $^{-2}$ s $^{-1}$. In agreement, Lehmer et al. (2012) found that the normal-galaxy number counts rise rapidly at the faint end, compared to those of AGN, and contribute $\approx 46\%$ of the number counts in the soft band found in the *Chandra* Deep Field-South. On the other hand, an increasing number of faint and high-redshift quasars is being discovered with infrared, optical and X-ray surveys (Moran et al. 2014; Marleau et al. 2014; Lemons et al. 2015), supporting the idea that black holes may have a stronger than expected contribution to the CXRB (Dijkstra et al. 2004; Madau & Haardt 2015).

Our understanding of the Universe, based on theoretical models and numerical simulations, suggests scenarios from which the excess of the soft X-ray background might naturally emerge. Current models show that the unresolved CXRB in the 0.5 – 2 keV band can be produced by faint point sources, either AGN or galaxies, with a possible additional contribution produced by truly diffuse components such as the intergalactic medium (IGM). In particular, Dijkstra et al. (2012) assumed a power-law X-ray spectral energy distribution (SED) of sources and varied their X-ray luminosity per unit star formation rate with redshift, showing that faint galaxies at redshifts up to $z = 10$ can fully account for the unresolved portion of the CXRB; Cappelluti et al. (2012) investigated the power spectrum of the unresolved CXRB in the soft band and interpreted the signal as a mixture of contributions from low-luminosity AGN ($\sim 20\%$), galaxies up to $z = 10$ ($\sim 25\%$), and thermal emission of the IGM ($\sim 55\%$), where the contribution of galaxies was modeled with a power-law SED and normalized using the observed X-ray luminosity function; Madau & Haardt (2015) showed that a population of high-redshift quasars and AGN with a piece-wise power-law SED (Haardt & Madau 2012) can explain $\sim 60\%$ of the unresolved CXRB at ~ 2 keV. The latter possibility is particularly interesting since, according to Madau & Haardt (2015), such a population of sources could also fully reionize hydrogen and helium if their UV emissivity is normalized to the recent results of Giallongo et al. (2015).

Naturally, it is tempting to explain the excess in the soft CXRB as a contribution of high-redshift X-ray sources (Christian & Loeb 2013; McQuinn 2012) in galaxies existing before the end of the epoch of reionization (EoR) at $z_{\text{re}} \sim 6-9$ (Becker et al. 2015; Ade et al. 2015). These galaxies emit UV and X-ray photons which ionize and heat the intergalactic gas. While UV radiation has a small mean free path in the neutral medium and, thus, reionizes gas close to the source (Wyithe & Loeb 2003), X-ray photons travel hundreds of comoving megaparsecs away, heating and partially ionizing the neutral gas far from the sources (Mirabel et al. 2011). In most of the currently discussed models of reionization, UV photons are more efficient than X-rays in ionizing the medium, and reionization proceeds inside-out down to the scale of the H II bubbles (Barkana & Loeb 2004), while X-rays only preheat the IGM. This picture, however, depends on the relative normalization of the two processes and there are scenarios in which X-rays are more efficient than

the UV photons in driving reionization, and it proceeds more homogeneously, with significant smoothing up to the typical X-ray mean free path (McQuinn 2012; Mesinger et al. 2013; Majumdar et al. 2015). The hardest X-rays emitted by a population of high-redshift sources are expected to have such large mean free paths that they are never absorbed by the IGM and, thus, contribute to the unresolved soft CXRB observed today.

The extent to which the first X-ray sources contribute to the CXRB, as well as their role in the thermal history and reionization of the IGM, depends on their nature. At present these sources are poorly constrained due to the lack of observations and there are several possible candidates, including X-ray binaries (XRB) (Power et al. 2009; Mirabel et al. 2011; Power et al. 2013; Fragos et al. 2013), mini-quasars (Madau et al. 2004), and hot gas in galaxies, hard photons emitted as a result of high-redshift supernovae activity (Oh 2001), as well as more exotic candidates such as annihilating dark matter (Cirelli et al. 2009). The spectral energy distribution of X-ray photons emitted in each case depends on the character of the sources, varying from a hard spectrum that peaks at the photon energy of ~ 3 keV, as in the currently favored case of XRBs (Mirabel et al. 2011; Fragos et al. 2013; Fialkov et al. 2014), to a soft power-law SED expected from hot gas heated by supernova explosions and winds within galaxies (e.g., Furlanetto (2006)).

The details of cosmic heating and reionization affect the redshifted 21-cm signal of neutral hydrogen (e.g., see Furlanetto et al. (2006); Pritchard & Furlanetto (2007); Ripamonti et al. (2008); Pritchard & Loeb (2012)). This radio signal, which is hoped to be the richest future probe of astrophysics and cosmology at high redshifts, is sensitive to the spectrum and nature of the early X-ray sources (Fialkov et al. 2014; Pacucci et al. 2014; Mirocha 2014; Fialkov & Barkana 2014; Fialkov et al. 2015; Ewall-Wice et al. 2016). In this paper we explore the redshifted 21-cm signal while constraining the luminosity of the high-redshift X-ray sources by the observed soft CXRB. The CXRB constraint yields an upper limit on the X-ray efficiency of each type of source and thus allows us to estimate the maximal possible effect of cosmic heating on the 21-cm signal. Such a limit has not been quoted before, although the effect of strong soft X-ray sources on the 21-cm signal has been studied (Pritchard & Loeb 2012; Mesinger et al. 2013; Pacucci et al. 2014). Moreover, we improve over the existing works by considering the CXRB limits on two new types of X-ray sources, namely, realistic X-ray binaries and mini-quasars, both with a hard SED. Given the great current uncertainty about the properties of early galaxies, this is an essential constraint that will help guide the search for the radio signal by existing, planned and upcoming radio telescopes designed to probe the 21-cm signal out to $z \sim 30$, such as the Square Kilometer Array (SKA, Koopmans et al. (2015)), The Hydrogen Epoch of Reionization Array (HERA)², Large Aperture Experiment to Detect the Dark Age (LEDA, Bernardi et al. (2016)), the Experiment to Detect the Global EoR Step (EDGES, Bowman & Rogers (2010)), the Dark Ages Radio Explorer (DARE, Burns et al. (2012)), the Shaped Antenna measurement of the background RA-

² <http://reionization.org/>

dio Spectrum (SARAS, Patra et al. (2013)), the SCI-HI experiment (Voytek et al. 2014), the Donald C. Backer Precision Array for Probing the Epoch of Reionization (PAPER, (Parsons et al. 2014)), Giant Metrewave Radio Telescope (GMRT, Paciga et al. (2013)), the Murchison Widefield Array (MWA, Bowman et al. (2013)), the LOw-Frequency ARray (LOFAR, van Haarlem et al. (2013)), and the New Extension in Nançay Upgrading LOFAR (NenuFAR, Zarka et al. (2012)).

The paper is organized as follows: in Section 2 we describe the simulation and model assumptions used in this work; in Section 3 we (1) use the observed unresolved CXRB to establish the upper bound on the X-ray efficiency of high-redshift sources, and (2) apply the existing upper limits on the 21-cm power spectrum to set the lower limit on the X-ray efficiency; in Section 4 we present our results for the thermal history, partial X-ray ionization, and the 21-cm signal; finally, we summarize and conclude in Section 5. Throughout this paper we use cosmological parameters as measured by the Planck Collaboration (Ade et al. 2013).

2 SIMULATED UNIVERSE

We simulated large cosmological volumes of 384^3 Mpc^3 of the high redshift Universe using a hybrid simulation, first introduced by Visbal et al. (2012) and described in detail by Fialkov et al. (2014); we describe it briefly here. Using the known statistical properties of the initial density field, we generated a random realization of the initial overdensity (with periodic boundary conditions) and the supersonic relative velocities between the gas and dark matter (Tsaliakhovich & Hirata 2010; Tsaliakhovich et al. 2011; Fialkov 2014) in a cubic volume. Given the large-scale density distribution, we then computed the gas fraction in star-forming halos in each cell as a function of time. In our simulation the star formation rate, found following the extended Press-Schechter formalism (Barkana & Loeb 2004), is modified by the large-scale density fluctuations and the supersonic relative velocities. Throughout the simulation we assume Population II stars with standard spectra [from Barkana & Loeb (2005); Leitherer et al. (1999)] and a star formation efficiency of 5%. We also account for the effect of photoheating feedback on the amount of gas available for star formation (Cohen et al. 2016a). Next, we use the stellar distribution to determine the X-ray heating rate, ionization, free electron fraction and the intensity of the Ly- α background in each cell. To this end, we first smooth the stellar density field at each redshift in shells around each cell. We assume the flux of X-ray and Ly- α photons emitted from each shell to be proportional to the star formation rate, which is in turn proportional to the time derivative of the amount of gas in star forming halos. We then compute the heating and ionization rates as well as the intensity of the Ly- α background by integrating over all the shells seen by each cell [using rates from Furlanetto & Stoever (2010)]. In this integral, the contribution of each cell to the rate at a given central cell is computed at the time-delayed redshift as seen by the central cell. Given the X-ray heating and ionization rates versus redshift at each cell, we integrated to get the gas temperature and free electron fraction as a function of time. To include UV reionization, we set each

cell to be fully reionized if some sphere around it contains enough ionizing photons to self-reionize (Furlanetto et al. 2004). With this simulation we followed the thermal history of the Universe and made predictions for the observable soft band CXRB and the 21-cm signal from a wide range of redshifts, $z = 6 - 40$, as discussed in Sections 3 and 4.

This tool, based on a combination of numerical simulation and analytical calculations has enough flexibility to explore various parameters of the unconstrained high redshift environment such as the X-ray efficiency (f_X) and SED of the first heating sources, the minimal mass of star forming halos and the reionization history. To probe the parameter space we consider two cases in which the IGM is reionized by UV photons emitted by early galaxies. In the “late reionization” case the Universe is fully reionized by $z_{\text{re}} = 6.2$, with the value of the electron optical depth falling in the range $\tau = 0.059 - 0.074$ which is within $1 - 2\sigma$ of the latest Planck result, $\tau = 0.058 \pm 0.012$, (Adam et al. 2016); while in the second case, “early reionization”, $z_{\text{re}} = 8.5$ and τ falls within $\sim 3\sigma$ of the Planck measurement. Late versus early reionization scenarios are obtained by varying the ionizing efficiency of sources in each model. When we normalize the X-ray emission (see below), we also use the redshift of full reionization as the cut-off time for this normalization; in this way, the two cases with different values of z_{re} also serve to probe which redshifts are really constrained by the X-ray background. Next, we consider two possible cases for the typical galactic halo mass: including star formation in halos down to the lowest mass that allows for efficient atomic cooling, which we term the “Atomic cooling” case, or adopting a minimum halo mass for star formation that is ten times larger (allowing for the possibility of strong feedback in small halos), which we refer to as “Massive halos”. Finally, we consider three types of X-ray sources: X-ray binaries that have a hard SED (Fragos et al. 2013; Fialkov et al. 2014), sources with a soft power-law SED of spectral index $\alpha_S = 0.5$ [where the luminosity L follows $dL/d\log\nu \propto \nu^{-\alpha_S}$] (Furlanetto 2006), and mini-quasars, i.e., central black holes in early star-forming galaxies, which we discuss in greater detail in Section 2.1.

The efficiency of hot gas or X-ray binaries is defined via the relation between the bolometric X-ray luminosity L_X and the star formation rate (SFR) of the galaxy

$$\frac{L_X}{\text{SFR}} = 3 \times 10^{40} f_X \text{ erg s}^{-1} \text{ M}_{\odot}^{-1} \text{ yr}^{-1}, \quad (1)$$

where the standard value of the X-ray efficiency is $f_X = 1$ (Furlanetto et al. 2006; Fragos et al. 2013). This relation is based on observations of nearby starburst galaxies and XRBs (Grimm et al. 2003; Gilfanov et al. 2004; Mineo et al. 2012a,b), and the standard normalization for XRBs (with $f_X = 1$) includes an order-of-magnitude increase in this ratio at the low metallicity expected for high-redshift galaxies (Fragos et al. 2013).

While the numerical factor in Eq.(1) was derived for X-ray binaries over the range 0.2 – 95 keV (Fragos et al. 2013), in this paper we chose a common normalization for soft and hard sources for simplicity. For easier comparison with other work in the literature, we list here the luminosities (for $f_X = 1$) in the 0.2–30 keV and 0.5–8 keV bands, for both the hard and the soft SEDs: $L_{0.2-30}^{\text{soft}}/\text{SFR} = 3 \times 10^{40}$, $L_{0.2-30}^{\text{hard}}/\text{SFR} = 2.8 \times 10^{40}$; $L_{0.5-8}^{\text{soft}}/\text{SFR} = 1.6 \times 10^{40}$,

$L_{0.5-8}^{\text{hard}}/SFR = 2.4 \times 10^{40}$. Note that in our late EoR scenario most of the X-rays that contribute to the CXRB originate near $z_{\text{re}} = 6.2$, in the rest-frame frequency range of 3.6 – 14.4 keV where the corresponding luminosities are $L_{3.6-14.4}^{\text{soft}}/SFR = 3.9 \times 10^{39}$ and $L_{3.6-14.4}^{\text{hard}}/SFR = 1.2 \times 10^{40}$. In the early EoR scenario, i.e., $z_{\text{re}} = 8.5$, *Chandra's* soft band probes the rest-frame 4.7 – 19 keV range where the luminosities amount to $L_{4.7-19}^{\text{soft}}/SFR = 3.4 \times 10^{39}$ and $L_{4.7-19}^{\text{hard}}/SFR = 8.7 \times 10^{39}$.

2.1 Mini-quasars

High redshift black holes are expected to be much lighter than the ones observed today in Milky Way size halos, $\sim 10^2 - 10^4 M_{\odot}$ compared to $\sim 10^6 - 10^9 M_{\odot}$. Until recently, the early population of high redshift black holes with such small masses was considered purely speculative. However, the latest observations find black holes with masses in the $10^2 - 10^6 M_{\odot}$ range in dwarf metal poor galaxies which may resemble the high-redshift environment. In particular, Moran et al. (2014) used the Sloan Digital Sky Survey to find 28 AGN in nearby low-mass, low-luminosity dwarf galaxies and estimated the minimum black-hole mass to fall mainly in the $10^3 - 10^4 M_{\odot}$ range, showing that AGN in dwarf galaxies are not as rare as previously thought; Marleau et al. (2014) studied the infrared signature of active nuclei in nearby dwarf galaxies and found black hole masses of $10^2 - 10^6 M_{\odot}$; while Lemons et al. (2015) found that relatively many hard X-ray sources in dwarf galaxies are ultra-luminous. The abundance and brightness of these sources suggest that mini-quasars and high redshift AGN may have had a stronger impact on reionization than what is usually assumed.

Here we use the internal feedback model for the black hole mass (Wyithe & Loeb 2003) and follow the discussion in Fialkov et al. (2014) to model the population of high redshift mini-quasars and their impact on the heating and reionization of the Universe. Thus, we find the ratio of the average X-ray luminosity of the central mini-quasar to that of XRBs in the same halo to be

$$\frac{L_{MQ}}{L_{XRB}} \sim 0.1 \left(\frac{0.05 f_X^{MQ}}{f_X f_{\star}} \right) \left(\frac{M_h}{10^8 M_{\odot}} \right)^{2/3} \frac{1+z}{10}, \quad (2)$$

where we assumed, as in the case of X-ray binaries, that on average 25% of the mini-quasar X-rays in the relevant wavelengths are not absorbed in the interstellar medium of the host galaxy. Here we needed this non-absorbed fraction in order to compare between XRBs (for whom ISM absorption is implicitly included in the spectrum, which is based on observations) to mini-quasars (for which we estimated the intrinsic emitted energy using a theoretical model). We note that, by using the XRB spectrum, we assume (like Fragos et al. (2013)) that this absorption at high redshifts is similar to that at the low redshifts of the observations. In the ratio in Eq. (1), f_X^{MQ} parameterizes the uncertainty in the X-ray efficiency of mini-quasars with $f_X^{MQ} = 1$ being its standard value. For simplicity, in the rest of this paper we omit the superscript MQ when talking about the X-ray efficiency of mini-quasars. Using Eq. (1) we can express the X-ray luminosity of a mini-quasar formed in a halo of mass M_h in terms of the star formation rate in the same halo.

Compared to XRBs, the X-ray luminosity of a mini-quasar is weighted by an additional factor of $(M_h/10^8 M_{\odot})^{2/3}$. Because of this additional factor, the contribution of mini-quasars to the X-ray background is expected to be negligible compared to that of XRBs at high redshifts ($z \gg 8$) where the typical halo mass is small, but it becomes important at lower redshifts ($z \ll 8$) at which larger halos form bigger black holes. When mini-quasar emission is modelled as a multi-colour Shakura & Sunyaev (1973) accretion disc, these sources are expected to have hard SEDs that are similar to those of XRBs, due to the weak dependence of the X-ray spectrum on the black hole mass (Tanaka et al. 2012). Therefore, we use the same SED for XRBs and mini-quasars in our calculation.

3 LIMITS ON THE X-RAY EFFICIENCY

In this work we rely on the observed intensity of the unresolved CXRB in the 0.5 – 2 keV band as measured by *Chandra* (Lehmer et al. 2012) to set the maximum possible X-ray efficiency for each type of the considered X-ray sources. Following the model developed by Cappelluti et al. (2012), we assume the extra-galactic contribution amounts to $2.51 \times 10^{-13} \text{ erg cm}^{-2} \text{ s}^{-1} \text{ deg}^{-2}$ and is provided solely by the pre-reionization sources. This normalization gives the maximal value of X-ray efficiency of the high-redshift heating sources that does not violate the observed soft band CXRB.

The values of f_X that we obtain by comparing the simulated background to the observed one are listed in the third column of Table 1 for each case of the reionization history and SED specified in the first two columns of the Table. We find that in order to produce the detected unresolved X-ray background, f_X must be 1–2 orders of magnitude larger than the standard value, $f_X \sim 1$, normally assumed in the literature for the efficiency of the high-redshift sources, although even higher values of f_X have been considered (Christian & Loeb 2013; Mesinger et al. 2013; Pacucci et al. 2014).

We find that hard sources, and in particular mini-quasars, are more efficient in producing the CXRB in the soft band, in that they require an X-ray efficiency that is a factor of a few lower than that of soft sources. This is because most of the energy emitted by soft X-ray sources redshifts to frequencies much lower than the observed band. Therefore, a high efficiency is needed in that case in order to increase the number of photons that eventually redshift into the relevant energy range. On the other hand, in the case of the hard X-ray sources (XRBs and mini-quasars) the SED peaks at ~ 3 keV and, at least for sources at $z \sim 6$ existing just before the end of reionization in our late reionization scenario, the observed 0.5 – 2 keV band probes the energy range around the peak of the SED, and a lower efficiency is sufficient to produce the observed CXRB.

Even though the maximum X-ray efficiencies that we find are relatively high, the population of pre-reionization sources with such efficiencies is still very dim and cannot be resolved into point sources by *Chandra*. In Figure 1 we show the cumulative number counts expected for such a population for the case of the high-redshift X-ray sources with a soft SED, with $f_X = 29.5$ (and $f_X = 1$ for comparison). As

Model	SED	f_X	z_h	x_{ion}^X	τ_{UV}	τ_{tot}	T_{21}^{min} [mK]	z_{min}	T_{21}^{max} [mK]	z_{max}
Massive	Hard	14.7	13.5	7.6%	0.0597	0.0609	-85.3	17.0	20.8	10.7
Late EoR	Soft	41.4	17.0	27.3%	0.0601	0.0688	-29.7	18.8	26.2	12.8
$z_{\text{re}}^{\text{UV}} = 6.2$	MQ	12.1	13.0	6.4%	0.0597	0.0606	-99.7	16.7	19.6	10.4
Massive	Hard	79.2	15.7	9.3%	0.0831	0.0850	-42.7	18.5	22.7	12.8
Early EoR	Soft	187.7	18.8	34.5%	0.0833	0.0934	-15.1	20.3	26.3	14.3
$z_{\text{re}}^{\text{UV}} = 8.5$	MQ	87.9	15.4	8.6%	0.0831	0.0847	-47.5	18.2	22.2	12.5
Atomic	Hard	10.8	16.2	10.5%	0.0739	0.0756	-107.4	20.6	23.0	13.0
Late EoR	Soft	29.5	20.1	40.0%	0.0746	0.0859	-48.8	22.7	29.7	15.6
$z_{\text{re}}^{\text{UV}} = 6.2$	MQ	11.4	14.0	7.5%	0.0738	0.0747	-147.4	19.3	17.7	11.6
Atomic	Hard	44.4	18.5	13.5%	0.0957	0.0990	-68.8	21.9	25.9	15.2
Early EoR	Soft	102.4	21.9	39.1%	0.0961	0.1111	-29.2	24.1	30.4	17.3
$z_{\text{re}}^{\text{UV}} = 8.5$	MQ	74.4	16.9	10.5%	0.0956	0.0977	-99.0	20.9	22.5	14.0

Table 1. For each scenario of structure formation and reionization (column 1; 4 total scenarios) we list the SED (column 2), f_X (column 3) set so that the high-redshift sources produce the entire unresolved CXRB in the 0.5–2 keV band of $2.51 \times 10^{-13} \text{ erg cm}^{-2} \text{ s}^{-1} \text{ deg}^{-2}$ (Cappelluti et al. 2012), the heating transition redshift z_h (column 4), the X-ray ionization fraction at the end of the UV reionization (column 5), the UV contribution to the optical depth (column 6) and the total optical depth τ_{tot} due to the UV and X-ray ionization (column 7), the minimal temperature of the global 21-cm signal (T_{21}^{min} , column 8), and the redshift at which it occurs (z_{min} , column 9), the maximal temperature of the global 21-cm signal in emission (T_{21}^{max} , column 10), and the redshift at which it occurs (z_{max} , column 11).

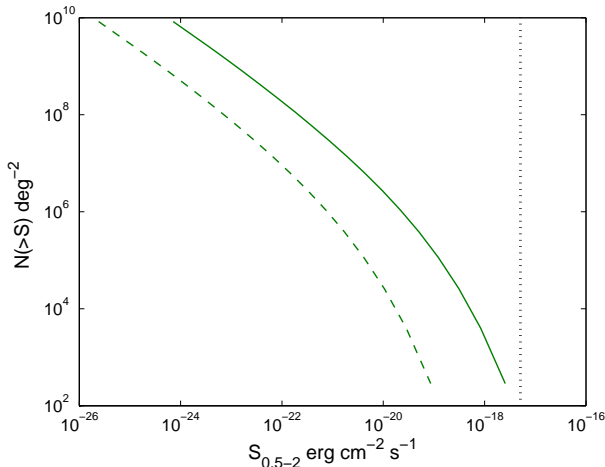


Figure 1. Cumulative X-ray number counts at $z = 6.2$ for the soft band with atomic cooling halos and a soft SED, for $f_X = 29.5$ (solid) or $f_X = 1$ (dashed). The vertical dotted line shows the detection limit of *Chandra* in the soft band.

we see from the Figure the fluxes are well below the detection limit of the satellite, $\sim 5.1 \times 10^{-18} \text{ erg cm}^{-2} \text{ s}^{-1}$, and, therefore, it is correct to consider these sources as unresolved ones, as we do in this work.

Another trend in the normalized X-ray efficiencies f_X in Table 1 is that the early reionization cases correspond to a higher f_X . This is not due to reionization itself but since (as noted in Section 2) we use the end of reionization as a convenient cutoff redshift for the X-ray source population, in order to probe how various redshifts are constrained. Thus, in the case of early reionization, when the X-ray sources that we are considering are assumed to be cut off below $z = 8.5$, we require a very high normalization at $z > 8.5$ in order to explain the observed CXRB. Another way to express this is

that sources at higher redshifts are less strongly constrained, i.e., a higher maximal f_X is allowed for them without violating the observed CXRB. The f_X values shown in Table 1 can be seen as upper limits on a hypothetical high-redshift population of X-ray sources that formed down to $z = 6.2$ or $z = 8.5$, and may have had a much higher X-ray efficiency than is typical for low-redshift galaxies. In the case of Massive halos, there are fewer galaxies at any given redshift than in the Atomic case, so the X-ray efficiency must be higher in order to explain the same, fixed, level of the observed CXRB.

The shape of the unresolved CXRB in the 0.5 – 2 keV band shown in Figure 2 is poorly constrained by observations, and only a general trend can be extracted from the available data at the moment. The best fit to *Chandra* data proposed by Hickox & Markevich (2006) is a power law with a spectral index of $\alpha = 0.5$ (but note that the amplitude of X-ray number counts, not the slope, was a free parameter in this fit). Another constraint on the shape of the CXRB comes from the data collected by the *Röntgenstrahlen* (ROSAT) satellite (Hasinger et al. 1993); McCammon et al. (2002) reported the spectral structure of the unresolved background measured in the $\sim 0.65 - 3.3$ keV range. These data were extracted after subtracting the local thermal component, the contribution of oxygen lines from the ROSAT data, and accounting for the AGN directly observed by the deep surveys with the satellite. However, due to a considerable discrepancy in the normalization of the CXRB measured by *Chandra* and ROSAT, which most likely arises from cosmic variance and systematics, it is unclear if the residual found in ROSAT data can be fully attributed to the cosmic background. Therefore, we only show the unresolved CXRB measured by ROSAT (black crosses in Figure 2) with its normalization re-scaled to the value of $2.51 \times 10^{-13} \text{ erg cm}^{-2} \text{ s}^{-1} \text{ deg}^{-2}$ in the 0.5 – 2 keV band.

Despite the discrepancy in the normalization and large uncertainties in the ROSAT data, it is still interesting to compare the shape of the CXRB found by McCammon et al.

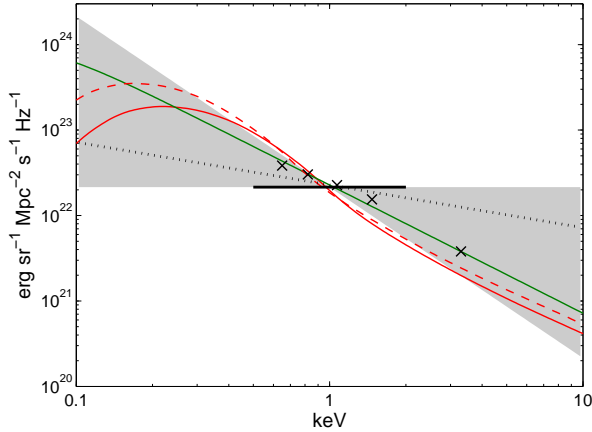


Figure 2. Extra-galactic contribution to the unresolved X-ray background in the 0.5 – 2 keV band versus the energy of the photon. Assuming atomic cooling halos, we show the cases of a hard spectrum for early (red dashed) or late (red solid) reionization; and a soft SED for early (green dashed) or late (green solid) reionization; the two soft SED cases lie on top of each other. We calibrate the CXRB in the soft band 0.5 – 2 keV to the value of $2.51 \times 10^{-13} \text{ erg cm}^{-2} \text{ s}^{-1} \text{ deg}^{-2}$ (Cappelluti et al. 2012), showing the average intensity with the black horizontal bar in the plot. We also show the shape of the “absolute” unresolved soft extragalactic X-ray background from McCammon et al. (2002) (crosses) normalized to the same value. The shaded area spans the range of slopes considered by Dijkstra et al. (2012) for the CXRB (between $\alpha = 0$ and $\alpha = 2$), and the black dotted curve has the best-fit spectral index from *Chandra* data (Hickox & Markevich 2006), $\alpha = 0.5$.

(2002) to what is extracted from our simulations (Figure 2). This shape is in good agreement with the CXRB which we get using our soft SED while our hard SED yields a slightly steeper frequency dependence; the fit to *Chandra* data is somewhat softer than predicted by our models. Because observational constraints on the slope are so poor and inconclusive, a wide variety of possible SEDs are considered in the literature when modeling high-redshift populations. For instance, Dijkstra et al. (2012) explored a wide range of spectral indices, $\alpha = 0 - 2$, of high-redshift galaxy SEDs when trying to reproduce the observed CXRB (this range is marked as the shaded area in Figure 2). Both our cases (soft and hard SEDs) yield a CXRB with slopes which (approximately) fall within this range. We note that our normalization at 0.5 – 2 keV is consistent with Moretti (2012), but their data suggest a somewhat harder spectrum towards higher energies than the range shown in Figure 2.

A lower limit on the X-ray efficiency can in some cases be extracted from the upper limit on the 21-cm power spectrum (Pober et al. 2015; Ali et al. 2015). As we will see in the next Section, the hotter is the IGM, the smaller is the amplitude of the 21-cm signal seen against the CMB. Consequently, a very cold IGM results in fluctuations of large amplitude that can be ruled out by existing observations. Parsons et al. (2014) were the first to place limits on X-ray heating with the 21-cm power spectrum using the data collected by the PAPER experiment. Current upper limit on the 21-cm power spectrum of $\sim 500 \text{ mK}^2$ at $z = 8.4$ in the range of wavenumbers $k = 0.15 - 0.5 \text{ h Mpc}^{-1}$ (Pober et al.

2015; Ali et al. 2015) yields $f_X \gtrsim 0.0095$ (0.0023) in the case of a hard (soft) SED for our atomic cooling case and $f_X \gtrsim 0.036$ (0.01) in the case of massive halos for the late EoR scenario. Our early reionization scenario is not constrained by this measurement since the universe is fully ionized by $z_{\text{re}} = 8.5$ and the 21-cm signal at lower redshifts vanishes for all heating scenarios.

4 RESULTS

4.1 Ionization and Heating

In this section we present our quantitative results for the possible consequences of having strong X-ray sources at high redshift as currently allowed by the CXRB. One obvious result is that X-ray sources with a high X-ray efficiency heat up the IGM much earlier than is normally expected. The moment when the gas heats up to the temperature of the CMB (the cosmic heating transition), of which redshift we denote z_h , happens earlier in the models where f_X is set to its upper limit compared to the predictions for the $f_X = 1$ case. In the case of the soft SED, late reionization and atomic cooling, this transition happens a $\Delta z_h = 5.3$ earlier, while in the case of XRBs the advance is $\Delta z_h = 4.2$. In Table 1 we list z_h for all the considered cases with the maximum f_X , while Table 2 shows the same cases but for $f_X = 1$.

It is interesting to see if the saturated heating assumption, which is often used in numerical simulations, holds during reionization when the CXRB limit is applied. Saturated heating is the assumption that the gas is much hotter than the CMB, i.e., $1 - T_{\text{CMB}}/T_K \sim 1$. If this assumption is valid, then the heating history can be ignored when reionization is considered. Considering our models with f_X values from Table 1, we find that in the case of a hard SED the value of the factor $1 - T_{\text{CMB}}/T_K$ is far from unity at the beginning of the EoR when the Universe is $\sim 5\%$ ionized. In particular in the case of late (early) reionization and atomic cooling, this factor (when averaged over a simulated box) is 0.6 (0.59) at $x_{\text{HI}} = 95\%$ for X-ray binaries and -0.36 (-0.1) for mini-quasars. In the case of late (early) reionization and massive halos, this factor is 0.66 (0.75) for X-ray binaries, and 0.5 (0.7) for mini-quasars. By the mid-point of UV reionization, $1 - T_{\text{CMB}}/T_K \gtrsim 0.95$ in all the simulated cases from Table 1 and, hence, the saturated heating assumption applies during the second half of reionization. The CXRB-normalized models with a soft SED yield $1 - T_{\text{CMB}}/T_K \gtrsim 0.97$ already at an ionization fraction of 5%.

Along with heating, X-rays partially ionize the neutral medium, competing with the UV photons in powering reionization. The efficiency of X-rays versus UV in ionizing the cosmic gas depends on the values of the escape fraction and the X-ray efficiency. Here we keep the former parameter fixed in each case by fixing the redshift at which reionization is completed by the UV photons, while varying the latter. In the standard case of $f_X = 1$, the main source of ionization is UV photons while X-rays are expected to yield only a small contribution, ionizing the gas only up to a few percent when reionization is completed by UV. To emphasize this, we list the level of the partial ionization by X-rays (within the final remaining neutral regions just before they are reionized), x_{ion}^X , at the end of reionization powered by UV photons, in

Model	SED	z_h	x_{ion}^X	T_{21}^{min} [mK]	z_{min}
Massive	Hard	9.7	0.7%	-167.7	14.9
Late EoR	Soft	12.2	2.3%	-121.3	16.1
$z_{\text{re}}^{\text{UV}} = 6.2$	MQ	9.5	0.6%	-174.3	14.6
Massive	Hard	9.6	0.2%	-163.9	14.9
Early EoR	Soft	12.1	0.5%	-120.9	16.1
$z_{\text{re}}^{\text{UV}} = 8.5$	MQ	9.3	0.1%	-171.7	14.6
Atomic	Hard	12.0	1.3%	-169.6	18.2
Late EoR	Soft	14.8	4.5%	-134.8	19.6
$z_{\text{re}}^{\text{UV}} = 6.2$	MQ	10.1	0.8%	-201.3	16.6
Atomic	Hard	12.0	0.5%	-169.6	18.3
Early EoR	Soft	14.8	1.6%	-134.7	19.7
$z_{\text{re}}^{\text{UV}} = 9$	MQ	10.0	0.2%	-202.9	16.5

Table 2. $f_X = 1$ case. For each scenario of structure formation and reionization (column 1), we show the SED (column 2), the heating transition redshift z_h (column 3), the X-ray ionization fraction at the end of the UV reionization (column 4), the minimal temperature of the global 21-cm signal (T_{21}^{min} , column 5), and the redshift at which it occurs (z_{min} , column 6).

the fourth column of Table 2. The value of x_{ion}^X does not rise above 4.5%.

On the other hand, with f_X set to its maximum by normalization to the CXRB, the X-ray efficiency is substantially higher and in some cases the X-rays start competing with UV in the quest for reionizing the Universe (see the x_{ion}^X column in Table 1). Partial ionization by X-rays is especially high in the case of the soft spectrum due to the extremely high X-ray efficiency in combination with the rapid, efficient absorption of soft X-rays by neutral gas. For instance, by the end of the UV reionization it reaches $x_{\text{ion}}^X \sim 40\%$ in the case of atomic cooling scenario. For XRBs and mini-quasars, x_{ion}^X grows to 13.5% and 10.5%, respectively, by the end of UV reionization (for the case of atomic cooling and early reionization). It is interesting to note that while UV photons heat and ionize the gas close to the source (given their very small mean free path within neutral gas), X-rays travel larger distances before inputting their energy in the IGM. As a result, in the extreme cases with high f_X , reionization is much more homogeneous, and may even proceed outside-in (Mesinger et al. 2013; Majumdar et al. 2015) instead of the conventional inside-out picture (Barkana & Loeb 2004).

4.2 21-cm signal

The brightness temperature of the 21-cm signal, observed with the CMB as a diffuse background source, is expected to be a three-dimensional probe of the high-redshift Universe. Current and planned telescopes are designed to measure the redshift evolution of this signal averaged over two-dimensional spheres (the global spectrum) as well as its spatial fluctuations at each given epoch which will allow us to extract the power spectrum. The predicted global spectrum contains information about milestones in the evolution of the Universe and for a wide range of models exhibits a prominent absorption trough which single-dish radio telescopes seek to observe. The sky-averaged brightness temperature reaches its minimal value at the point when heating sources turn on and begin raising the temperature

of the IGM towards T_{CMB} . The power spectrum at each comoving wavenumber, k , when plotted as a function of redshift, shows a sequence of peaks driven by various spatially and temporally varying physical quantities (such as the kinetic gas temperature, fraction of neutral gas, and intensity of Ly- α radiation) which determine the intensity of the 21-cm transition. A generic plot of this type for the 21-cm power spectrum has three peaks (Barkana & Loeb 2005; Pritchard & Furlanetto 2007; Pritchard & Loeb 2008): the high-redshift peak, at $z \sim 20 - 30$, is due to Ly- α fluctuations; the mid-redshift peak, which is due to heating fluctuations, appears at $z \sim 15 - 22$, but this peak is not present on scales below the X-ray mean free path (Fialkov & Barkana 2014); and the low-redshift peak, at $z \sim 7 - 10$, is due to ionization fluctuations. of the main targets of the present-day and future radio interferometers.

In Figures 3 (for the late reionization scenario) and 4 (which assumes early reionization) we plot the global spectrum of the 21-cm signal and its spherically-averaged power spectrum, with the X-ray efficiencies normalized to the CXRB as well as the cases with $f_X = 1$, $f_X = 0$ and $f_X = 1000$ shown for comparison. The latter case (which we shown only for the soft SED) clearly over-produces the observed CXRB, while the case of $f_X = 0$ and late reionization is excluded by the PAPER observations. We do show these cases to demonstrate the effect of either extremely strong or absent X-ray heating (the excluded cases are shown with black lines in Figures 3 and 4). In addition, for the late reionization scenario and hard SED shown in Figure 3 we demonstrate the 21-cm signal with the lowest possible X-ray efficiencies (red dotted lines) normalized to the current PAPER limits (black triangle) as discussed at the end of Section 3. Finally, we plot the expected thermal noise power spectrum of phase 1 of the SKA assuming a single beam, an integration time of 1000 hours, and a 10 MHz bandwidth. In the case of global 21-cm experiments, in principle, short integration times (minutes) suffice to detect the signal with a single dish (Shaver 1999). In practice, though, the need for accurate calibration and precise removal of the spectrally smooth foreground make these measurements quite difficult, especially given the complex coupling of the errors at different frequencies. Quantitative analyses show that if calibration can remove any sharp frequency response, then it is possible to overcome the issues of a smooth foreground and thermal noise, and global signals such as those we predict in this paper should be detectable (Pritchard & Loeb 2010; Liu et al. 2013; Morandi & Barkana 2012; Bernardi et al. 2016).

We find that the cases of enhanced heating of the IGM strongly affect the expected global 21-cm signal. In particular, because the gas does not have sufficient time to cool down prior to being heated by X-rays, the absorption trough becomes shallower and thus harder to observe, requiring a higher precision of calibration and longer integration times. For instance, in the case of late reionization and atomic cooling, the minimal brightness temperature is reduced by $\sim 64\%$ for a soft SED and $\sim 37\%$ for a hard SED. In addition, the absorption trough is shifted to lower frequencies: from 70 MHz to 60 MHz ($\Delta z \sim 3.1$) in the case of the soft SED, from 74 MHz to 66 MHz ($\Delta z \sim 2.4$). Finally, with the enhanced heating the emission signal is much stronger and the peak shifts to higher redshifts; for each model the maximal possible value of the emission signal is realized

when the normalization is set so as to produce the full unresolved CXRB. In particular, in the case of late reionization and atomic cooling, the maximal brightness temperature is boosted by a factor of ~ 2 (~ 1.6) for XRBs (hot gas). See Tables 1 and 2 for more information.

As discussed above, X-rays speed up reionization and the intensity of the 21-cm signal drops faster than otherwise expected towards the end of the reionization era, which is most noticeable in the cases with soft X-rays and maximal efficiency (set to the full CXRB), as well as in the excluded case of extreme heating (with $f_X = 1000$) where reionization ends considerably earlier than in other models. In addition, Ly- α photons generated by X-rays in the neutral IGM through relaxation of hydrogen atoms excited by primary photoelectrons are boosted by a factor of f_X in each case. For $f_X = 1$ these photons are far less important than Ly- α directly generated by stars; however, for $f_X \sim \mathcal{O}(100)$ the contribution of these two sources becomes comparable. In this case, the 21-cm signal couples to the temperature of the gas (Wouthuysen 1952; Field 1958) earlier than it would for $f_X = 1$, which can be seen in Figures 3 and 4 for the cases with soft X-rays and CXRB normalization as well as the extreme heating case.

One of the striking consequences of the high X-ray efficiency on the power spectrum is that the amplitude of the 21-cm fluctuations is suppressed at high redshifts ($\sim 15 - 25$), making their detection from this epoch harder. In particular, the Ly- α peak at $z \sim 25$ may become unobservable in the case of the soft SED. This happens mainly because the Ly- α fluctuations are anti-correlated with fluctuations seeded by inhomogeneous heating (prior to the heating transition), which is partially compensated by the enhanced generation of Ly- α photons by X-ray excitation of the IGM. In most cases, there remains a significant signal from cosmic dawn observable with the SKA, even in these worst-case scenarios (in terms of observing cosmic dawn). Comparing the three cases of $f_X = 1$, $f_X = 29.5$ and $f_X = 1000$ with a soft SED, atomic cooling and late EoR, we see that the Ly- α peak drops from 95 mK^2 at $z = 22.6$ ($f_X = 1$) to 17 mK^2 at $z = 25.6$ ($f_X = 29.5$) and to 12 mK^2 at $z = 28.6$ ($f_X = 1000$). The effect of X-rays on the heating peak in the 21-cm power spectrum is also dramatic. The heating peak is lower and is shifted to higher redshifts (lower frequencies) when X-rays are strong. In the just-considered case of soft X-rays, atomic cooling and late EoR, the heating peak drops from 304 mK^2 at $z = 16.9$ ($f_X = 1$) to 155 mK^2 at $z = 21$ ($f_X = 29.5$) to 70 mK^2 at $z = 24.7$ ($f_X = 1000$). Thus, when the X-ray SED is soft, the normalization to the full unresolved CXRB yields a lower limit for the amplitude of the Ly- α and X-ray heating peaks in the 21-cm power spectrum and an upper limit for the redshift at which these peaks are located. In the case of a hard SED, the main effect of X-rays is to suppress the Ly- α peak, as the fluctuations in temperature are washed out by the large mean free paths of the X-ray photons and the heating peak is not always present. The intensity of the 21-cm fluctuations from lower redshifts ($z \sim 10$) depends on both reionization and heating and, thus, is less straightforward to relate to the nature of the X-ray sources. In some cases the fluctuations are enhanced, because the heating is closer to being saturated during the reionization era; in others the fluctuations are suppressed as a result of the X-ray contribution to reionization.

Heating sources with extremely low X-ray efficiencies do not have enough time to heat the IGM before the end of reionization, and in this case the gas remains colder than the CMB even at that time. As a result, the absorption trough in the global spectrum is very deep, and the power spectrum features only two peaks sourced by inhomogeneous Ly- α and ionizing backgrounds. The latter peak is so strong in the case of $f_X = 0$ that it can be ruled out using current upper limits on the 21-cm power spectrum at $z = 8.4$ from PAPER as we have discussed at the end of Section 3. The minimal possible 21-cm brightness temperature reaches the value of $T_{21} = -231.7 \text{ mK}$ (-237.3 mK) at $z_{\min} = 14.2$ (12.5) for atomic cooling (massive halos) with a late EoR and $T_{21} = -218.6 \text{ mK}$ (-224.6 mK) at $z_{\min} = 15.2$ (12.8) for atomic cooling (massive halos) with an early EoR.

An intriguing result of our study is that, once available, the 21-cm global signal can be combined with the X-ray background produced by high-redshift sources to put constraints on the SED of these sources. Because hard sources are more efficient in seeding the CXRB, the CXRB limit implies a deeper 21-cm trough (as the Universe is colder) than is possible in the case of soft X-ray sources. In particular, focusing on our case of the atomic cooling halos and late EoR, we see that given the level of the X-ray background, the absorption trough in the case of XRBs reaches at least -107.4 mK , which is much deeper than the corresponding limit in the case of the soft X-rays, -48.8 mK . Therefore, observing a trough shallower than -107.4 mK would rule out such a population of X-ray sources with a hard SED. In the future, with the direct high-redshift X-ray observations of X-ray Surveyor or Athena and the observed global 21-cm at hand, it will be possible to significantly constrain the properties of the high redshift sources even without using any additional information. This method thus provides an important alternative to probing the nature of X-ray sources with the 21-cm power spectrum (Pritchard & Furlanetto 2007; Pacucci et al. 2014; Fialkov et al. 2015; Ewall-Wice et al. 2016). Moreover, having at hand the CXRB together with both the global 21-cm signal and its power spectrum can help to break degeneracies between X-ray heating and other model parameters. We leave a more detailed discussion of this to future work.

Finally, based on the whole ensemble of models considered here, it is possible to define a border line of the parameter space within which the 21-cm signal can vary without violating any existing observational constraints. For instance, from the data presented in this paper we see that the absorption trough of the global signal cannot be shallower than -15 mK or deeper than -238 mK , and it is located between $z = 12.5$ and $z = 24.1$. This border line can be used to guide future observations. Because the bank of models presented in this paper is limited, a more detailed discussion of this idea can be found in Cohen et al. (2016b) and our future work.

5 CONCLUSIONS

The main results of this paper are the consequences of the upper limit on the X-ray efficiency which various high-redshift hard or soft X-ray sources may have without violating the observed soft unresolved X-ray background. This

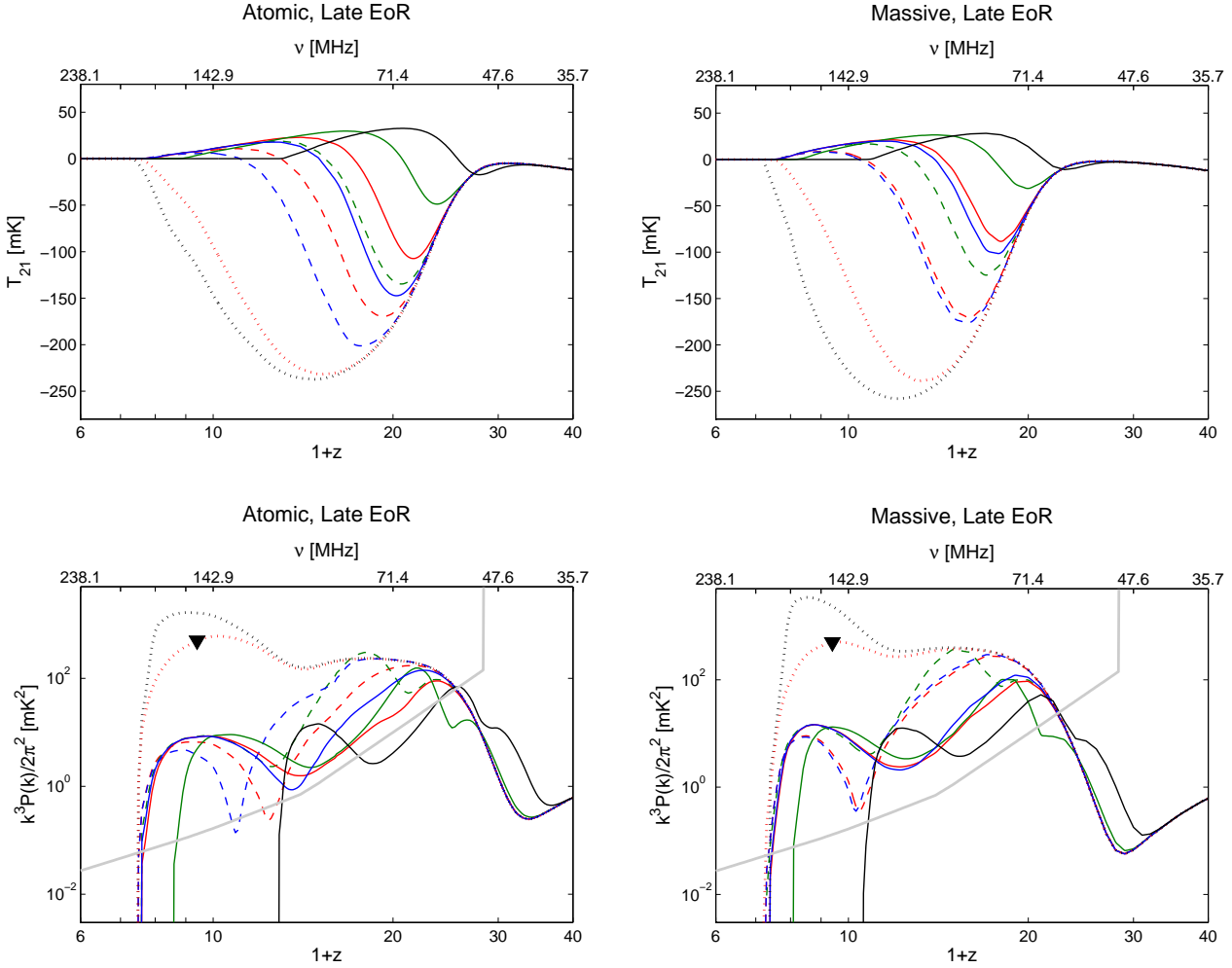


Figure 3. Global 21-cm brightness temperature (top) and its power spectrum in mK^2 units at $k = 0.2 \text{ Mpc}^{-1}$ (bottom) are shown for the atomic (left) and massive (right) cases for our late reionization case ($z_{\text{re}}^{\text{UV}} = 6.2$). We show the cases of X-ray sources with a soft SED (green), XRBs with a hard SED (red), or mini-quasars (blue), each for $f_X = 1$ (dashed) or f_X normalized to its maximum value based on the CXRB (solid). The red dotted line shows the case with a low heating efficiency of $f_X = 0.0095$ (0.036) for atomic cooling (massive halos) with a hard X-ray SED. The black triangle marks the upper limit on the 21-cm power spectrum at $z = 8.4$ (Pober et al. 2015) and the black dotted line shows the case of no heating, $f_X = 0$, which has been ruled out by this observation. In both the atomic and massive cases the black solid line shows the case of extreme heating ($f_X = 1000$, soft SED) which over-predicts the CXRB. Finally, the thick grey line shows the power spectrum of the thermal noise for phase 1 of SKA-low assuming a single beam, 1000-hour integration time, and a 10 MHz bandwidth.

limits allows us to estimate the maximal effect that early X-ray sources can have on the high-redshift 21-cm signal, reionization, the CMB, and the thermal history of the early Universe. Our results are particularly useful in light of the existing and upcoming radio telescopes designed to probe these early epochs.

We find that different types of high-redshift X-ray sources considered here (i.e., X-ray binaries, hot gas, or mini-quasars) naturally produce an X-ray background with a slope close to that of the observed unresolved soft CXRB, which, however, is poorly constrained by present observations. Therefore, it is hard to reach strong conclusions about the nature of X-ray sources based on the current measurements of the shape of the CXRB. On the other hand, normalization to the X-ray background does constrain the maximum possible X-ray efficiency which the high redshift heat-

ing sources can have. Hard X-ray sources are more efficient in producing the observed background, compared to the soft sources, and so the maximal X-ray efficiency is typically around 2–3 times lower for hard sources than for the soft ones. More generally, the X-ray efficiency that is needed to explain the CXRB is very high compared to what is normally assumed based on low redshift observations. This allows for a possibility that the high-redshift sources may be more luminous than their low-redshift counterparts. For a population of X-ray sources assumed to have existed down to redshift 6.2 (and then cut off), this enhancement factor varies between ~ 10 and ~ 40 , for the various cases; for a population that only existed at $z = 8.5$ and above, the factor is in the range $\sim 44 - 190$.

Based on our most extreme case (the early reionization scenario with massive halos only), we can put a realistic up-

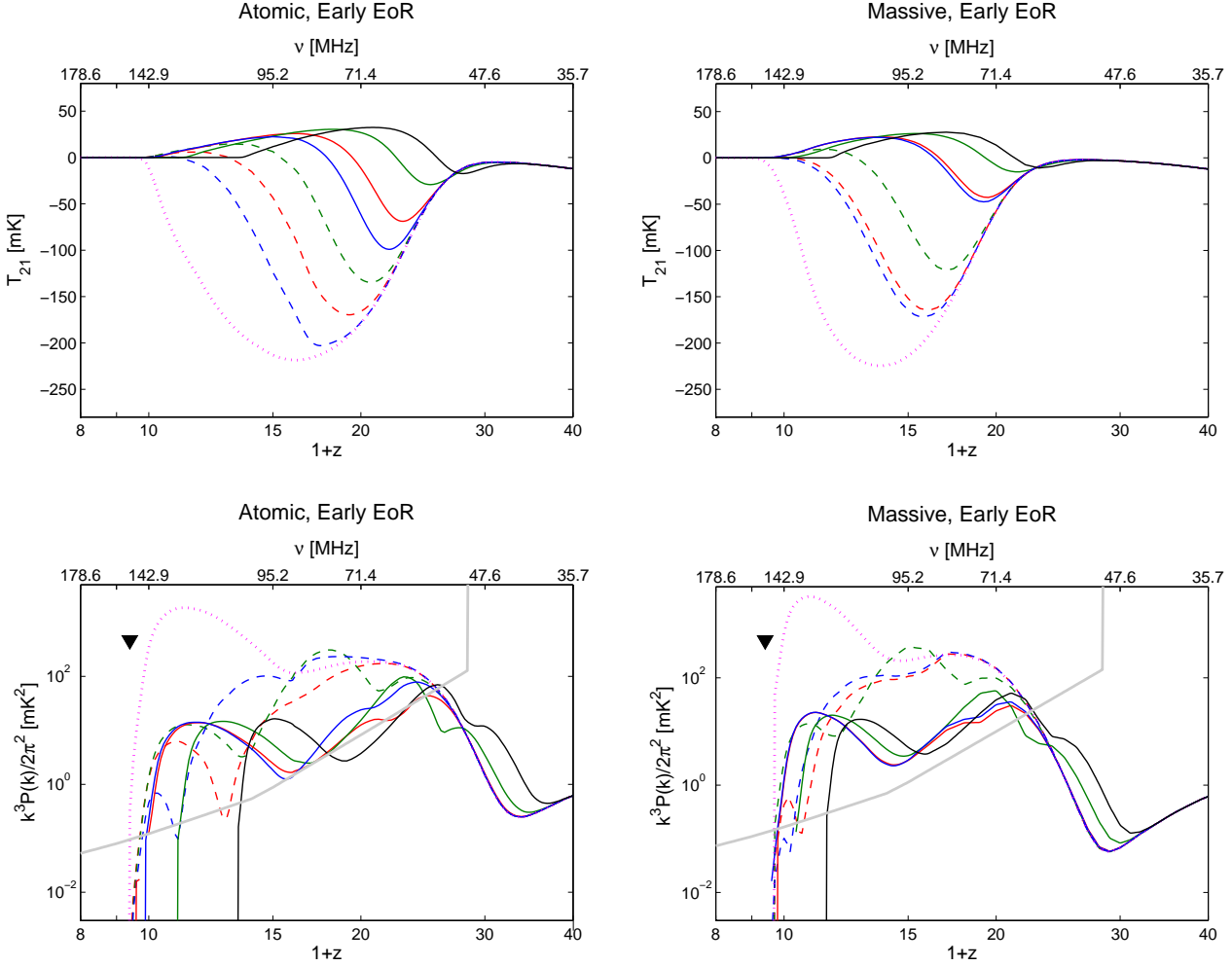


Figure 4. Global 21-cm brightness temperature (top) and its power spectrum in mK^2 units at $k = 0.2 \text{ Mpc}^{-1}$ (bottom) are shown for the atomic (left) and massive (right) cases for our early reionization case ($z_{\text{re}}^{\text{UV}} = 8.5$). We show the cases of X-ray sources with a soft SED (green), XRBs with a hard SED (red) or mini-quasars (blue), each for $f_X = 1$ (dashed) or f_X normalized to its maximum value based on the CXRB (solid). The magenta dotted line shows the case with no heating, i.e., $f_X = 0$. The black triangle marks the upper limit on the 21-cm power spectrum at $z = 8.4$ (Pober et al. 2015). In both the atomic and massive cases the black solid line shows the case of extreme heating ($f_X = 1000$, soft SED) which over-predicts the CXRB. Finally, the thick grey line shows the power spectrum of the thermal noise for phase 1 of SKA-low assuming a single beam, 1000-hour integration time, and a 10 MHz bandwidth.

per bound on the bolometric luminosity of the high-redshift sources per star formation rate: $\sim 2.4 \times 10^{42} \text{ erg s}^{-1} \text{ M}_{\odot}^{-1} \text{ yr}$ for XRBs, $\sim 5.6 \times 10^{42} \text{ erg s}^{-1} \text{ M}_{\odot}^{-1} \text{ yr}$ in the case of hot gas, and $\sim 2.6 \times 10^{42} \text{ erg s}^{-1} \text{ M}_{\odot}^{-1} \text{ yr}$ for mini-quasars (assuming the luminosity - SFR relation of proportionality). Interestingly, recent observations suggest that hard X-ray sources such as X-ray binaries or accreting black holes are a factor of ~ 10 more luminous in metal-poor than in solar-metallicity galaxies (Prestwich et al. 2013; Brorby et al. 2014). In addition, X-ray sources in low-redshift dwarf galaxies appear to be ultra-luminous (Lemons et al. 2015). However, these trends would have to greatly increase in order to approach the upper bounds that we find.

The possible enhanced heating at high redshift has direct implications for the thermal history and the reionization of the IGM as well as for the 21-cm signal produced by neutral hydrogen during and prior to cosmic reionization. In

particular, cosmic heating can happen up to $\Delta z \sim 4-5$ earlier than what is normally assumed. However, even with the enhanced X-ray emission the saturated heating assumption throughout reionization can only be used with soft sources. In addition, efficient X-ray sources compete with stellar sources in ionizing the gas. In particular, X-ray sources with soft spectra can be so efficient as to compete with UV photons in reionizing the Universe, producing a fractional increase in the optical depth to CMB photons of 12 – 16%. In the cases when X-rays are so efficient, reionization happens more homogeneously since X-rays have a very long mean free path compared to UV and, thus, ionize the IGM far from the sources. On the other hand, hard sources such as XRBs and mini-quasars (with their maximal normalization) have only a mild effect on reionization, producing a fractional increase in the CMB optical depth of only 1 – 3%.

Thus, in our model reionization is mainly driven by

stellar sources which emit UV, while quasars can have a small impact on the EoR channeling their energy into hard X-rays. A different situation was described recently by Madau & Haardt (2015) who explored a possibility of reionization achieved only by high redshift quasars and other faint, high-redshift AGN. Madau & Haardt (2015) assigned a composite emissivity to their quasars accounting for a broad spectrum of emitted photons, from optical to hard X-rays (Haardt & Madau 2012), which resulted in a stronger contribution of AGN to reionization. These authors found that $z > 5$ active galaxies can reionize the universe without overproducing the unresolved CXRB at 2 keV (amounting to $\sim 60\%$ of the CXRB) provided their properties are similar to those of their lower redshift counterparts. The contribution of high redshift quasars in this case was normalized by fitting the observed integrated optical emissivity at redshifts up to ~ 5 (Bongiorno et al. 2007; Schulze 2009; Giallongo et al. 2015) and extrapolating this result to higher redshifts out to $z \sim 12$. This emissivity drops slowly with redshift, predicting a significant population of quasars at early times. Based as it is on the extrapolation of current scarce high-redshift observations, this result may overestimate the role of quasars and AGN in reionization.

An important implication of the possible high X-ray efficiency of the early X-ray sources is the signature that they imprint in the 21-cm signal of neutral hydrogen. This signal has not been detected yet, and its discovery is a major goal of the astronomical community. Since the agents of high-redshift cosmic heating are highly unconstrained, a wide space of possibilities is left for the 21-cm signal, which translates into a wide parameter space for telescopes to search. Having an upper limit on the effects of cosmic heating naturally constrains the search parameter space and can help guide telescope design and search strategies. An upper limit on heating has important implications both for the global spectrum and for the spatial fluctuations of the 21-cm signal.

In the case of a high X-ray efficiency, the absorption trough of the global 21-cm signal is significantly reduced and shifted towards lower frequencies (higher redshifts), while the reionization gradient (in emission) is extended over a broader range of frequencies. The 21-cm power spectrum is suppressed at high redshifts ($z \sim 15 - 25$) due to the enhanced heating, and the Ly- α peak is reduced and shifted to lower frequencies as well as the X-ray peak (if present); however, the fluctuations from the second half of reionization are maintained and sometimes boosted due to the effect of saturated heating. Thus, there is mixed news for 21-cm experiments. For global experiments, the expected signal from reionization and cosmic dawn is bounded and for some models can be significantly reduced. For phase 1 of the SKA, reionization remains observable at a high signal-to-noise ratio in all cases, but cosmic dawn can become difficult to observe in the most extreme cases. We note that in our calculation we do not account for exotic processes, such as dark matter annihilation, which could heat up the gas early on and suppress the 21-cm signal without leaving any X-ray background.

For completeness, we have also considered lower limits on the X-ray heating efficiency for late reionization scenarios (which do not end before $z = 8.4$) using recent upper limit found by PAPER. Weak or no X-ray heating results in a 21-cm signal with a deep absorption trough in the global signal

and strong fluctuations from all the epochs that normally have a signal that is suppressed due to cosmic heating. Such a signal should be an easy target for radio telescopes.

To summarize, the unknown details of star formation, the process of reionization and the nature of high-redshift X-ray sources, including their SED and X-ray efficiency, result in a large uncertainty in the expected 21-cm signal. Specifically, the absorption trough, the main feature of the global 21-cm signal, can vary in depth anywhere from $T_{21} \sim -240$ mK to -15 mK, and in position from $z \sim 12$ to 24; the fluctuation peak from mid-reionization is still unconstrained to better than the range of 3-3000 mK² at $k = 0.2$ Mpc⁻¹; the X-ray peak strongly depends on the properties of the X-ray sources and can be strong, mild or vanishing; finally, the strength of the fluctuation peak from the Ly- α coupling era varies between 2 and 200 mK² and its redshift lies within $z \sim 13 - 25$.

While the CXRB narrows the possible realization space of the 21-cm background only slightly at present, future X-ray missions such as Athena and X-ray Surveyor could directly probe high redshift sources of X-rays, constraining their effect on the intergalactic gas and the 21-cm signal.

6 ACKNOWLEDGMENTS

We thank L. V. E. Koopmans for providing the noise spectrum of SKA and A. Vikhlinin for his input on the CXRB. We also thank the anonymous referee for carefully reading our work and providing valuable comments.

A. F. was partially supported by the LabEx ENS-ICFP: ANR-10-LABX-0010/ANR-10-IDEX-0001-02 PSL. R.B. and A.C. acknowledge Israel Science Foundation grant 823/09 and the Ministry of Science and Technology, Israel. R.B.'s work has been done within the Labex Institut Lagrange de Paris (ILP, reference ANR-10-LABX-63) part of the Idex SUPER, and received financial state aid managed by the Agence Nationale de la Recherche, as part of the programme Investissements d'avenir under the reference ANR-11-IDEX-0004-02. R.B. also acknowledges a Leverhulme Trust Visiting Professorship; this research was also supported in part by Perimeter Institute for Theoretical Physics. Research at Perimeter Institute is supported by the Government of Canada through Industry Canada and by the Province of Ontario through the Ministry of Economic Development & Innovation. J.S. was supported by the ERC Project No. 267117 (DARK) hosted by Universite Pierre et Marie Curie (UPMC) - Paris 6, PI J. Silk. JS acknowledges the support of the JHU by NSF grant OIA-1124403.

REFERENCES

- Ade, P. A. R., et al., 2014, *A&A*, 571, 16
- Ade, P. A. R., et al., 2016, *A&A*, 594, 13
- Adam, R., et al., 2016, arXiv:1605.03507
- Ali, Z. S., Parsons, A. R., Zheng, H., Pober, J. C., Liu, A., et al. 2015, *ApJ*, 809, 61
- Barkana R., Loeb A., 2004, *ApJ*, 609, 474
- Barkana, R., & Loeb, A. 2005, *ApJ*, 626, 1
- Bauer, F. E., Alexander, D. M., Brandt, W. N., et al., 2004, *AJ*, 128, 2048

- Becker, G. D., Bolton, J. S., Madau, P., et al., 2015, *MNRAS*, 447, 3402
- Bernardi, G., Zwart, J. T. L., Price, D., et al. 2016, *MNRAS*, 461, 2847
- Bongiorno, A., Zamorani, G., Gavignaud, I., et al., 2007, *A&A* 472, 443
- Bowman, J. D., & Rogers, A. E. E., 2010, *Nature*, 468, 796
- Bowman, J. D., Cairns, I., Kaplan D. L., Murphy, T., Oberoi, D., et al., 2013, *PASA*, 30, 031
- Brorby, M., Kaaret, P., & Prestwich, A. 2014, *MNRAS*, 441, 2346
- Burns, J. O., Lazio, J., Bale, S., Bowman, J., Bradley, R., et al., 2012, *AdSpR*, 49, 433
- Cappelluti, N., Ranalli, P., Roncarelli, M., Arevalo, P., Zamorani, G., et al., 2012, *MNRAS*, 427, 651
- Christian, P., Loeb, A., 2013, *JCAP*, 09, 014
- Cirelli, M., Iocco, F., Panci, P., 2009, *JCAP*, 10, 009
- Cohen, A., Fialkov, A., Barkana, R., 2016a, *MNRAS*, 459, 90
- Cohen, A., Fialkov, A., Barkana, R., 2016b, arXiv:1609.02312
- Dijkstra, M., Haiman, Z., & Loeb, A. 2004, *MNRAS*, 613, 646
- Dijkstra, M., Gilfanov, M., Loeb, A., Sunyaev, R., 2012, *MNRAS*, 421, 213
- Ewall-Wice, A., Hewitt, J., Mesinger, A., Dillon, J. S., Liu, A., Pober, J., 2016, *MNRAS*, 458, 2710
- Fialkov, A., Barkana, R., Visbal, E., 2014, *Nature*, 506, 197
- Fialkov, A. & Barkana, R., 2014, *MNRAS*, 445, 213
- Fialkov, A., 2014, *IJMPD*, 2330017
- Fialkov, A., Barkana, R. & Cohen, A., 2015, *PRL*, 114, 1303
- Field, G. B., 1958, *Proc. Institute Radio Engneers*, 46, 240
- Fragos, T., Lehmer, B. D., Naoz, S., Zezas, A., Basu-Zych, A., 2013, *ApJ*, 776, 31
- Furlanetto, S. R., Zaldarriaga, M., Hernquist, L., 2004, *ApJ*, 613, 1
- Furlanetto, S. R., Oh, S. P., Briggs, F. H., 2006, *PhR*, 433, 181
- Furlanetto, S. R., 2006, *MNRAS* 371, 867
- Furlanetto, S. R., Stoeber, S. J., 2010, *MNRAS* 404, 1869
- Giacconi, R., Gursky, H., Paolini, F., Rossi, B., 1962, *PRL*, 9, 439
- Giallongo, E., Grazian, A., Fiore, F., et al., 2015, *A&A* 578, A83
- Grimm, H.-J., Gilfanov, M., Sunyaev, R., 2003, *MNRAS*, 339, 793
- Gilfanov, M., Grimm, H.-J., Sunyaev, R., 2004, *MNRAS*, 347, 57
- Haardt, F. & Madau, P., 2012, *ApJ*, 746, 125
- Hasinger, G., Burg, R., Giacconi, R., Hartner, G., Schmidt, et al., 1993, *A&A*, 275, 1
- Hickox R. C., Markevitch M., 2006, *ApJ*, 645, 95
- Koopmans, L., Pritchard, J., Mellema, G., Aguirre, J., Ahn, K., et al., 2015, *AASKA14*, 1
- Liu, A., Pritchard, J. R., Tegmark, M., Loeb, A., 2013, *PRD*, 87, 3002
- Leitherer, C., Schaerer, D., Goldader, J. D., Delgado, R. M. G., Robert, C., et al., 1999, *ApJS*, 123, 3
- Lehmer, B. D., Xue, Y. Q., Brandt, W. N., Alexander, D. M., Bauer, F. E., et al., 2012, *ApJ*, 752, 46L
- Lemons, S. M., Reines, A. E., Plotkin, R. M., Gallo, E., Greene, J. E., 2015, *ApJ*, 805, 12
- Madau, P., Rees, M. J., Volonteri, M., Haardt, F., Oh, S. P., 2004, *ApJ*, 604, 484
- Madau, P. & Haardt, F., 2015, *ApJ*, 813, 8
- Majumdar, S., Jensen, H., Mellema, G., Chapman, E., Abdala F. B., 2016, *MNRAS*, 456, 2080
- Marleau, F. R., Clancy, D., Bianconi, M., Habas, R., 2014, arXiv:1411.3844
- McCammon, D., Almy, R., Apodaca, E., Bergmann Tiest, W., Cui, W., et al., 2002, *ApJ*, 576, 188
- McQuinn, M., 2012, *MNRAS*, 426, 1349
- Mesinger, A., Ferrara, A., Spiegel, D. S., 2013, *MNRAS*, 431, 621
- Mineo, S., Gilfanov, M., Sunyaev, R., 2012a, *MNRAS*, 426, 1870
- Mineo, S., Gilfanov, M., Sunyaev, R., 2012b, *MNRAS*, 419, 2095
- Mirabel, I. F., Dijkstra, M., Laurent, P., Loeb, A. & Pritchard, J. R., 2011, *A&A* 528, A149
- Mirocha, J., 2014, *MNRAS*, 443, 1211
- Moran, E. C., Shahinyan, K., Sugarman, H. R., Velez, D. O., Eracleous, M., 2014, *AJ*, 148, 136
- Morandi, A., Barkana, R., 2012, *MNRAS*, 424, 2551
- Moretti, A., Vattakunnel, S., Tozzi, P., et al. 2012, *A&A*, 548, A87
- Oh, S. P., 2001, *ApJ*, 553, 499
- Paciga, G., Albert, J. G., Bandura, K., Chang, T.-C., Gupta, Y., et al., 2013, *MNRAS*, 433, 639
- Pacucci, F., Mesinger, A., Mineo, S., Ferrara, A., et al., 2014, *MNRAS*, 443, 678
- Parsons, A. R., Liu, A., Aguirre, J. E., Ali, Z. S., Bradley, R. F., et al., 2014, *ApJ*, 788, 106
- Patra, N., Subrahmanyan, R., Raghunathan, A., Udaya Shankar, N., 2013, *ExA*, 36, 319
- Pober, J. C., Ali, Z. S., Parsons, A. R., McQuinn, M., Aguirre, J. E., et al. 2015, *ApJ* 809, 62
- Power, C., Wynn, G. A., Combet, C., Wilkinson, M. I., 2009, *MNRAS*, 395, 1146
- Power, C., James, G., Combet, C., Wynn, G., 2013, *ApJ*, 764, 76
- Prestwich, A. H., Tsantaki, M., Zezas, A., et al., 2013, *ApJ*, 769, 92
- Pritchard, J. R. & Furlanetto, S. R. 2007, *MNRAS*, 376, 1680
- Pritchard, J. R. & Loeb, A., 2008, *PRD*, 78, 3511
- Pritchard, J. R. & Loeb, A., 2010, *PRD*, 82, 023006
- Pritchard, J. R. & Loeb, A., 2012, *RPP*, 75, 6901
- Ripamonti, E., Mapelli, M., Zaroubi, S., 2008, *MNRAS*, 387, 158
- Schulze, A., Wisotzki, L., & Husemann, B., 2009, *A&A* 507, 781
- Shakura N. I., Sunyaev R. A., 1973, *A&A*, 24, 337
- Shaver, P. A., Windhorst, R. A., Madau, P., de Bruyn, A. G., 1999, *A&A*, 345, 380
- Tanaka, T., Perna, R., Haiman, Z., 2012, *MNRAS*, 425, 2974
- Tselikhovich D., Barkana R., Hirata C. M. 2011, *MNRAS*, 418, 906
- Tselikhovich D., Hirata C. M., 2010, *PRD*, 82, 083520
- van Haarlem, M. P., Wise, M. W., Gunst, A. W., Heald, G., et al., 2013, *A&A* 556, 2
- Visbal, E., Barkana, R., Fialkov, A., Tselikhovich, D., &

- Hirata, C. M., 2012, *Nature*, 487, 70
- Voytek, T. C., Natarajan, A., Jáuregui García, J. M., Peterson, J. B., & López-Cruz, O. 2014, *ApJL*, 782, L9
- Weisskopf, M. C., Gaskin, J., Tananbaum, H. & Vikhlinin, A., 2015, *SPIE*, 9510, 02
- Wouthuysen, S. A., 1952, *AJ*, 57, 31
- Wyithe, J. S. B., Loeb, A., 2003, *ApJ*, 595, 614
- Wyithe, J. S. B., Loeb, A., 2003, *ApJ*, 586, 693
- Xue, Y. Q., Luo, B., Brandt, W. N., et al., 2011, *ApJS*, 195, 10
- Zarka, P., Girard, J. N., Tagger, M., & Denis, L. 2012, SF2A-2012: Proceedings of the Annual meeting of the French Society of Astronomy and Astrophysics